UNDER REVIEW

RESCIENCE C

Replication / Computational Neuroscience

[Re] Context-Dependent Encoding of Fear and Extinction Memories in a Large-Scale Network Model of the Basal Amygdala

Tawan T. A. Carvalho[1], Luana B. Domingos[2], Renan O. Shimoura[3], Nilton L. Kamiji[3], Vinicius L. Cordeiro[4], Mauro Copelli[1], and Antonio C. Roque[3]

[1]Department of Physics, Federal University of Pernambuco, Recife, PE, Brazil – [2]Department of Pharmacology, Ribeirão Preto Medical School (FMRP), University of São Paulo, Ribeirão Preto, SP, Brazil – [3]Department of Physics, School of Philosophy, Sciences and Letters of Ribeirão Preto (FFCLRP), University of São Paulo, Ribeirão Preto, SP, Brazil – [4]Systems Neuroscience Institut (INS, UMR 1106), Aix-Marseille University, Marseille, France

Edited by
(Editor)

Received
01 March 2021

Published
–

DOI
–

Copyright © 2021 T. T. A. Carvalho and L.B. Domingos and R. Shimoura and N.L. Kamiji and V.L. Cordeiro and M. Copelli and A. C. Roque, released under a Creative Commons Attribution 4.0 International license.
Correspondence should be addressed to Tawan T. A. Carvalho (tawantayron@yahoo.com.br)
The authors have declared that no competing interests exists.
Code is available at https://github.com/tawantayron/RE-Fear-and-extinction-in-a-BA-net-model..

Introduction

The basal nucleus of the amygdala (BA) plays a central role in context-dependent fear associations [1], and computational modeling constitutes an important tool to understand the mechanisms involved. A neural network model of the basal amygdala could be used to simulate the differential recruitment of two distinct subpopulations of neurons during conditioning and extinction of fear memory [2]. Differential activation of neurons may result from the simultaneous association of the conditioned and unconditioned stimuli ($CS - US$) in the conditioning context, and weakened association in the extinction context. For a specific context, neurons are stimulated by different contextual inputs (CTX) [1]. Vlachos et al. [2] developed two models to study this dynamics in the BA: a mean-field model and a large-scale network of leaky integrate-and-fire (LIF) neurons with conductance-based synapses. The original implementation used MATLAB for the mean-field model and the NEST simulator [3] for the spiking network model. Here, we reimplemented the models using Python and the Brian 2 simulator [4], and provided information about parameter values and simulation conditions not explicitly described in the main article.

Methods

In the present work we replicate the main results from Vlachos et. al. [2]. In this section, we explain the details of the implementations of the two models. We start by describing the mean-field model, then we move to the spiking network model and the measures and methodological procedures adopted in the original work. Here, we refer to the $CS - US$ input as only CS, since there is no explicit distinction between them in the reference work.

Mean-field model

The mean-field model is described by a Wilson-Cowan type rate dynamics [5], and consists of two neural populations with dynamics described by

$$\tau_i \frac{dR_i}{dt} = -R_i + \xi(t) + (k_i - r_i R_i)\Phi(I_i), \tag{1}$$

where the subindex i ($i \in \{\mathrm{A}, \mathrm{B}\}$) indicates the neural population, R_i is the time-dependent population firing rate, ξ is a Gaussian white noise input $\xi(t) = \mathcal{N}(\mu, \sigma)$, k_i is the maximum firing rate, r_i is the refractoriness parameter, and Φ is the transfer function defined by

$$\Phi(x) = \frac{1}{1 + e^{-p(x-\theta)}}. \tag{2}$$

The function in Equation 2 is a sigmoid with values in the range $[0, 1]$, and the parameters p and θ determine its steepness and point of maximum slope, respectively. The input received by population i is represented by I_i, and consists of synaptic and external inputs,

$$I_i = \underbrace{w_{ij} R_j}_{\text{synaptic}} + \underbrace{w_{\mathrm{i,CS}} CS_i + w_{\mathrm{i,CTX}} CTX_i}_{\text{external}}, \tag{3}$$

where, w_{ij} indicates the weight of the synaptic connection from population j to i. CS_i and CTX_i are the conditioning and contextual inputs to population i with their respective synaptic weights $w_{\mathrm{i,CS}}$ and $w_{\mathrm{i,CTX}}$.
The CS input consists of a sequence of short square pulses of 50 ms duration each, and the CTX input is a longer square pulse applied continuously. When CTX is active for population i it is silent for population j and vice-versa (see Figure 1).

The weight $w_{\mathrm{i,CTX}}$ is fixed but the weight $w_{\mathrm{i,CS}}$ varies with time according to the following learning rule

$$\frac{dw_{\mathrm{i,CS}}}{dt} = \alpha_i CS\, CTX_i, \tag{4}$$

where α_i is the learning rate. All parameters used in the simulations of the mean-field model are shown in Table 1.

Table 1. Parameters of the mean-field model (Equations 1- 4) used in our simulations.

Rate model parameters		
Steepness of Φ	p	1.2 s
Maximum slope of Φ	θ	2.8 Hz
Maximum firing rate	k_i	0.97 Hz
Refractoriness parameter	r_i	10^{-3}
Learning rate	α	0.15 s
CS input strength	CS	0.5
CTX input strength	$CTX_{A,B}$	0.3
CTX synaptic weight	w_{CTX}	1.0
Initial CS synaptic weight	w_{CS}	1.0
Population coupling synaptic weight	w_{ij}	-1.0

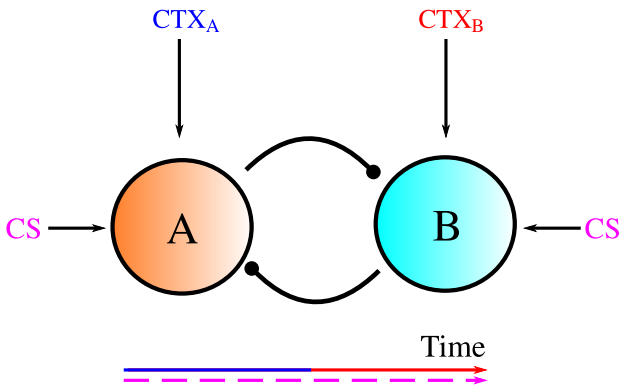

Figure 1. Schematic representation of the mean-field model. Populations A and B are mutually synaptically connected. The two populations receive the same CS input (short pulses), and population A receives a CTX_{A} continuous input and population B receives a CTX_{B} continuous input. The colored time axis indicates when each of such stimuli is active. Excitatory connections are represented by arrows and inhibitory ones by circles.

Spiking network model

Neurons of the spiking network model were described by the leaky-integrate-and-fire (LIF) model. The subthreshold dynamics of neuron i is given by

$$\frac{dv^i}{dt} = \left(G_l\left(E_0 - v^i\right) + G^i_{exc}\left(E_{exc} - v^i\right) + G^i_{inh}\left(E_{inh} - v^i\right)\right)/C_m, \tag{5}$$

where v^i is the membrane potential, G_l is the membrane (leakage) conductance, G_{exc} is the total excitatory synaptic conductance, G_{inh} is the total inhibitory synaptic conductance, E_0 is the resting potential, E_{exc} is the reversal potential of the excitatory synapse, E_{inh} is the reversal potential of the inhibitory synapse, and C_m is the membrane capacitance [6]. When $v^i(t) \geq \theta$, where θ is the spike threshold, the neuron emits a spike and the voltage is reset to E_k and remains fixed at this value for a refractory period

τ_{ref}. The parameters of the neuron model in Equation 5 are given in Table 2. In the simulations, the initial conditions of the voltages v of all neurons were drawn from a normal distribution with mean E_0 and standard deviation 3.0 mV.

Table 2. Parameters of the spiking neuron model (Equation 5) used in our simulations (extracted from [6]).

Spiking neuron parameters		
Membrane conductance	G_l	16.7 nS
Resting potential	E_0	-70.0 mV
Reset voltage	E_k	-70.0 mV
Excitatory synaptic reversal potential	E_{exc}	0.0 mV
Inhibitory synaptic reversal potential	E_{inh}	-80.0 mV
Membrane capacitance	C_m	250.0 pF
Spike threshold	θ	-50.0 mV
Refractory period	τ_{ref}	2.0 ms

The network is composed of 4,000 neurons, of which $N_E = 3,400$ are excitatory and $N_I = 600$ are inhibitory. The neurons are randomly connected with probabilities that depend on the types (exc or inh) of the pre- and postsynaptic cells. Synapses from a neuron onto itself (autapses) are allowed. The connection probabilities are given in Table 3.

Table 3. Probabilities of the four types of connections between neurons and their respective synaptic weights. The synaptic weights are drawn from normal distributions with mean μ and standard deviation σ [2] as indicated in the table.

Connection type	Probability		Synaptic weights	
Excitatory to excitatory	p_{EE}	0.01	μ = 1.25 nS	σ = 0.1 nS
Excitatory to inhibitory	p_{IE}	0.15	μ = 1.25 nS	σ = 0.1 nS
Inhibitory to excitatory	p_{EI}	0.15	μ = 2.50 nS	σ = 0.1 nS
Inhibitory to inhibitory	p_{II}	0.10	μ = 2.50 nS	σ = 0.1 nS

The synaptic conductances obey the equations

$$\frac{dG}{dt} = G_{aux} - \frac{G}{\tau_r}, \tag{6}$$

$$\frac{dG_{aux}}{dt} = -\frac{G_{aux}}{\tau_d} + W\delta(t - t' - D), \tag{7}$$

where G is used to represent either G_{exc} or G_{inh}, G_{aux} is an auxiliary variable, and τ_r and τ_d are the rise and the decay time constants, respectively. We will use $\tau_r = \tau_d = 0.326$ ms [6], so that G is an alpha function.
In Equation 7, W is the synaptic weight added to the variable G_{aux} at time t due to a spike in the presynaptic neuron at time t', and D is the transmission delay from pre- to postsynaptic neuron. The value of D is drawn from a normal distribution with mean $\mu = 2$ ms and standard deviation $\sigma = 0.1$ ms. The value of the synaptic weight W depends on the type of synapse and is indicated in Table 3.

Spiking network inputs

Besides recurrent connections from other network neurons, each neuron of the spiking network model receives three kinds of input: background (BKG), consisting of 1,000 inputs per neuron representing external synapses received from neurons in other brain areas; conditioned stimulus (CS), consisting of short pulses of 50 ms of duration; and

Table 4. Parameters (rates of Poisson processes and synaptic weights) and types of synaptic inputs applied to the network neurons. The weights of all BKG and CS to INH (inhibitory neurons) inputs are fixed, while the weights of the CS to EXC (excitatory neurons) and CTX inputs are plastic and have their initial values drawn from normal distributions with parameters (mean μ and standard deviation σ) indicated in the table.

Inputs parameters			
Connection	Type	Rate	Weight
BKG to EXC	Static	5 Hz	1.25 nS
BKG to INH	Static	6 Hz	1.25 nS
CS to INH	Static	500 Hz	$\mu = 0.9$ nS, $\sigma = 0.1$ nS
CS to EXC	Plastic	500 Hz	$\mu = 0.9$ nS, $\sigma = 0.1$ nS
CTX to subpop. A/B	Plastic	300 Hz	$\mu = 0.4$ nS, $\sigma = 0.05$ nS

contextual input (CTX). All these inputs are modeled as excitatory synapses activated by independent Poisson processes with specific rates.
The rates of the BKG inputs to excitatory and inhibitory neurons are distinct. These rates were adjusted so that the baseline network spiking activity was lower than 1 Hz for excitatory neurons and between 10-15 Hz for inhibitory neurons, as observed experimentally [7]. The rates of the CS and CTX inputs are the same for all neurons. The input rates and their respective synaptic weights are shown in Table 4.
To model conditioning and extinction of fear memories in the BA, two subpopulations of excitatory neurons containing 20% of N_E, i.e. 680 neurons, were chosen without overlap. The first subpopulation (pop_A) represents the fear neurons which receive context$_A$ input (CTX_A), and the second (pop_B) represents the extinction neurons which receive context$_B$ input (CTX_B).
Figure 2 shows all the inputs described above with emphasis on subpopulations A and B that are formed exclusively by excitatory neurons. The first stage of the simulation represents the conditioning phase in which CTX_A and CS are activated (CTX_B is deactivated), and the second stage represents the extinction phase, in which CTX_B and CS are activated (CTX_A is deactivated).

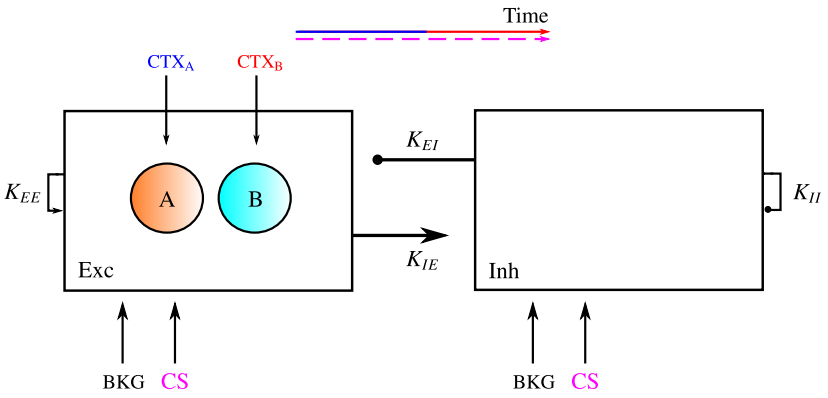

Figure 2. Schematic diagram of the spiking network model. Excitatory and inhibitory populations are represented by rectangles with the two excitatory subpopulations (A and B) that receive CTX inputs highlighted as colored circles. The excitatory and inhibitory populations receive BKG and CS (short pulses) inputs and the subpopulations A and B receive aditional CTX_A and CTX_B inputs, respectively. The colored time axis indicates when CTX_A and CTX_B inputs are active. Excitatory connections are represented by arrows and inhibitory ones by circles.

Table 5. Synaptic plasticity parameters

Synaptic plasticity		
Learning rates	α_1, α_2	1.6×10^{-3}
Neuromodulator present/absent	m	0 or 1
Maximum value of synaptic weight	w_{max}	4.0 nS
Mininum value of synaptic weight	w_{min}	0.4 nS
Time constant for variable c	τ_c	10 ms
Time constant for variable h	τ_h	10 ms
Increment to variable c	c_u	0.35
Increment to variable h	h_u	0.35

Plasticity

The synaptic weights of all network connections are static, except the ones of the connections from the CS and CTX inputs to the excitatory neurons, which are modified according to the following phenomenological rule:

$$w_+ = \begin{cases} w_- + \alpha_1 \cdot h \cdot m \cdot c \cdot |w_{max} - w_-| & \text{if } CS \text{ and } CTX \text{ temporally overlap} \\ w_- - \alpha_2 \cdot m \cdot c \cdot |w_{min} - w_-| & \text{otherwise,} \end{cases} \tag{8}$$

where w_- is the synaptic weight before the update, w_+ is the synaptic weight after the update, α_1 and α_2 are the learning rates, w_{max} (w_{mim}) is the maximum (minimum) value of the synaptic weight, m is a binary number that represents the action of a neuromodulator, and c and h are auxiliary variables that encode the recent activity in the synapse that receives input from CS and CTX, respectively.
The overlap described in Equation 8 refers to when there is a temporal superposition of CS and CTX inputs for the same neuron on a time window of up to 100 ms. If the temporal overlap occurs, the synapses that connect the CS and CTX to the target neuron are strengthened; otherwise, both synapses are weakened.
The dynamics of the variables c and h are described by

$$\dot{c} = -\frac{c}{\tau_c} + c_u \cdot \delta(t - t_{pre-CS}) \tag{9}$$

$$\dot{h} = -\frac{h}{\tau_h} + h_u \cdot \delta(t - t_{pre-CTX}), \tag{10}$$

where τ_c and τ_h are time constants and c_u (h_u) is an increase in variable the c (h) when a spike is emitted by the CS (CTX) source at $t = t_{pre}$. The values of the parameters used to model synaptic plasticity are shown in Table 5.

Simulation protocols

In this section we define the protocols used for the simulations of the spiking network model. In all cases described below, the BGK input is always active.

Spontaneous Activity — The network was simulated only with the BKG input during 1 second to evaluate the spontaneous activity generated by the model.

Dynamics of conditioning and extinction processes — After 50 ms of initial transient period, the conditioning phase begins with the activation of the input CTX_A and the application of 5 CS pulses (50 ms each) intercalated at intervals of 150 ms. After CTX_A is turned

off, a transient period of 100 ms follows and the same protocol is repeated for CTX_B but with 6 CS pulses instead of 5.
During each presentation of CS (both in the conditioning phase and in the extinction phase), the variable m in Equation 8 takes the value 1, and otherwise the value 0. Thus, the synaptic weights CS and CTX vary during the simulation due to synaptic plasticity, starting with the initial values given in Table 4.

Fear renewal — The fear renewal stage starts by repeating the previous protocol followed by the reactivation of CTX_A at the end of the extinction phase, together with a single presentation of the CS.

High connectivity introduces gamma oscillations — In this protocol the p_{ii} (see Table 3) is increased from 0.1 to 0.5 and only the conditioning phase is activated with the application of 10 CS pulses.

Blockage of inhibition — This protocol follows the same procedure described in *Dynamics of conditioning and extinction processes*, but two different conditions are simulated: either 50% or 90% of inhibitory neurons are deactivated during the extinction phase.

Measures

In this section we show how the measures used in our replication of the original study are defined:

- Throughout the simulation, we recorded the firing times for the construction of raster plots of neuronal activity.
- During CS presentations to pop_A and pop_B, we counted the total number of spikes in each subpopulation and divided it by the CS duration (50 ms) to calculate the average firing rate.
- We recorded the time series of CS and CTX synaptic strengths to pop_A and pop_B throughout the simulations. With that, we calculated the averages of these weights separately during each presentation of CS.
- The population spiking activity is the average spike count within a time window $\Delta t = 1$ ms, unless otherwise stated.
- We estimated the power spectrum density (PSD) of the population spiking activity using the Welch's method (from python package *SciPy*).
- The synchrony index was calculated as the variance of the population spiking activity divided by its mean. This measure is a simplification of the normalized synchrony index introduced by Golomb and Rinzel [8, 9].

Important information needed during replication

The general information necessary for the replication done here was available in the original article. However, some details were not found neither in the reference paper nor in the supplementary material. Here we list these details and describe the considerations we made to replicate the results.

Missing parameter values —

- Almost every parameter for the mean-field model is not present in the original work, namely the strength of the CS and CTX inputs, w_{ij}, and w_{CTX}.
- The values of the spiking neuron parameters τ_m, E_0, E_{exc}, E_{inh}, θ and E_K in Equation 5 are said to be given in Table S1F of the supplementary material of the reference [2] paper. However, the only parameter value given in Table S1F is the one of τ_{ref}. The value of θ is given in the caption of Figure 5 as -57 mV and the other are missing. Furthermore, the initial value of v is not mentioned.
- The synapse model used is defined in the main text only as a conductance-based synapse with no mention to the conductance dynamics. Looking at the supplementary material, we found that the conductance time-course was described by a difference of exponentials. The equation is described in Table S1G [2] but is not cited in the main text. Nevertheless, the values of the parameters τ_r, τ_d and t_{peak} are not given.
- Some parameters are also not given in the main text for the synaptic plasticity model described by equations 6-8. These parameters are: w_{max}, w_{min}, A, B, τ_c and τ_h. Moreover, but less important, parameters α_1 and α_2 are written in Table S1H as a_1 and a_2.
- Table S1I from the supplementary material [2] defines BKG current injections to excitatory and inhibitory neurons) with DC and AC amplitude values. However, there is no information about the frequency or phase for the AC currents.
- In Figures 5, 7, and 8 of the original work [2], the authors used spike activity histograms to obtain the firing rate time series that characterize the population activity. However, the bin sizes used are different and not informed.
- The *High connectivity introduces gamma oscillations* protocol adopted in the original article was not clear if only the conditioning phase was considered, and the number of CS presentations was not specified.

Approximations done to replicate the results —

- In the mean-field model we considered the inputs CS and $CTX_{A/B}$ as square pulses with the same heights as used for the spiking network model (500 and 300 Hz, respectively), but we divided them by 1000 so that they remain below 1. We considered the synaptic weights as unitary, i.e., $w_{i,CS} = w_{i,CTX} = -w_{ij} = 1$.
- The neuron model equation used in the original text (Equation 5 of [2]) has a dimensional inconsistency. By reviewing the references cited by the authors, we found our Equation 5 in reference [6], which describes the same neuronal dynamics. We adopted this equation here with the same parameters given in [6] and shown in Table 2.
- The description of the synaptic model was also extracted from reference [6], where the synaptic conductances are given by a difference of exponentials with $\tau_r = \tau_d = 0.326$ ms. To implement the difference of exponentials in Brian 2, it was necessary to use two ordinary differential equations as shown in Equations 6 and 7.
- Due to the lack of details on the application of AC and DC currents to model the BKG input, we opted for the use of Poisson train generators (Table 4), which promoted a spontaneous activity compatible with what was experimentally expected [7].

- To replicate the results obtained in the evolution of synaptic weights, we used the values of CS and CTX shown in Table 4, which differ from those described in the supplementary material of the reference article [2].
- In Equations 9 and 10, we named the parameters c_u and h_u instead of A and B as in the reference article [2] to avoid misunderstandings in relation to subpopulations A and B. We also specified in these equations t_{pre-CS} and $t_{pre-CTX}$, which indicate when increments in auxiliary variables occur.
- In assessing how the increase in network connectivity introduces gamma oscillations, the authors did not clearly show how the frequency of population activity and the synchrony index were determined. In our replication, we used PSD to check the frequency of oscillations in the spiking activity of the network and chose population Fano Factor as the synchrony index.
- In Figure 9, we used 10 CS presentations which was the minimum number of presentation necessary to reproduce the original result.

Results

In this section, we present the results obtained from our simulations as described in Methods, which qualitatively reproduce the main results of the reference article.

Mean-field model

Despite the lack of information provided by the authors for this model, we have reproduced qualitatively the expected dynamics for the conditioning and extinction phases as shown in Figure 3**A**.
The external inputs CS and CTX were generated beforehand for the whole simulation time (Figure 3**C**). Therefore, we studied the evolution of the synaptic weights $w_{A/B,CS}$ by simply using the stimuli arrays and Equation 4 without simultaneously simulating the inputs. The synaptic weights evolution in Figure 3**B** is in accordance with what was reported in the reference paper (Figures 4C-D of [2]).

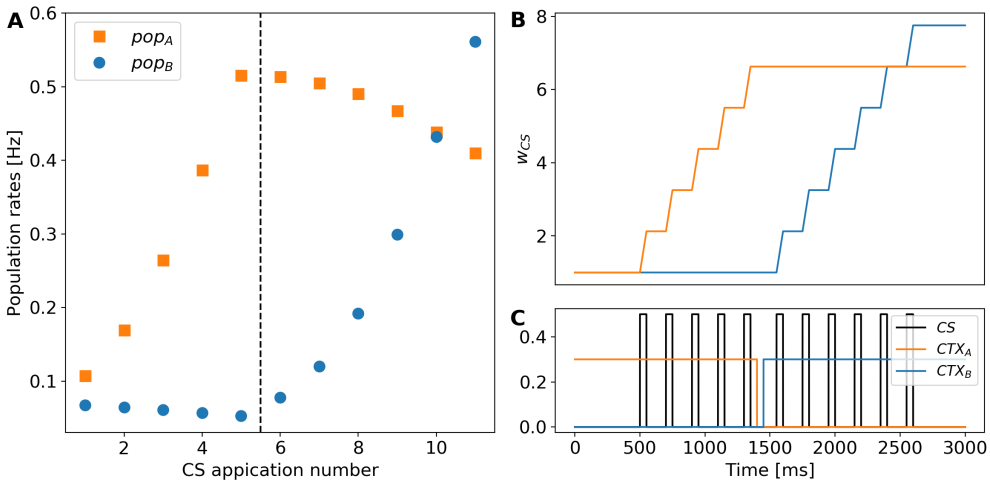

Figure 3. Dynamics of the mean-field model.(**A**) Firing rates of pop_A and pop_B at each CS application. The vertical red dashed line marks the transition from application of CTX_{A} to CTX_{B}. (**B**) Time evolution of $w_{A,CS}$, and $w_{B,CS}$. (**C**) Time evolution of the external inputs CS, CTX_A, CTX_B.

Spiking neuron network model of BA

Spontaneous Activity — In Figure 4 we show the raster plot of the simulated spontaneous activity of the network. The firing rates measured were 0.03 and 10.54 Hz per neuron for the excitatory and the inhibitory populations, respectively. This is compatible with the firing rates observed experimentally [7]. This consistency test was not presented in the original work.

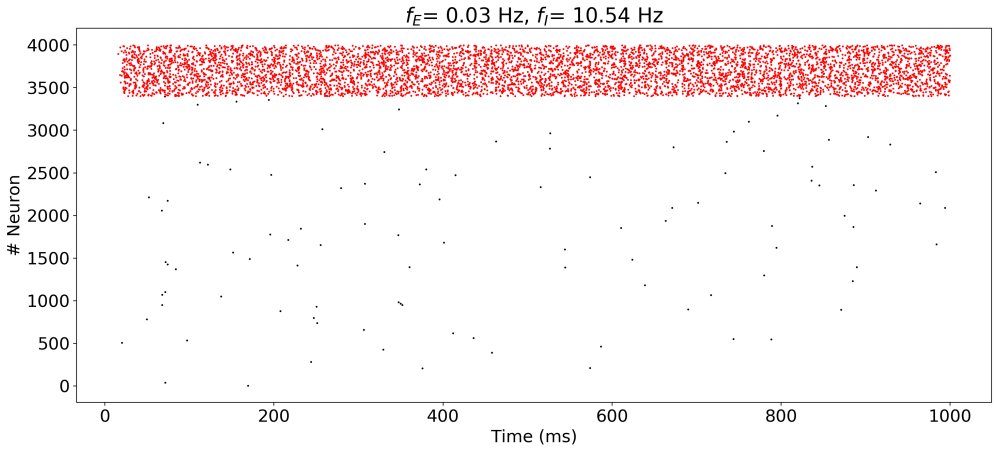

Figure 4. Raster plot of network spiking activity when there is only background input as external stimulus. The red dots represent spikes from the inhibitory population and the black dots represent spikes from the excitatory population.

Dynamics of conditioning and extinction processes — In Figure 5**A** we show the raster plot of spiking activity during the conditioning and extinction processes. The activities of subpopulations A and B, which represent fear and extinction neurons, respectively, are highlighted. After each presentation of CS during the conditioning phase, there is an increase in the firing rate of pop_A. On the other hand, in the extinction phase, after the first presentations of CS the pop_A firing rate gradually decreases while the firing rate of pop_B increases (Figure 5**B**). During these phases, the activity of the inhibitory neurons slightly fluctuated for each presentation of CS as shown in Figure 5**C**.

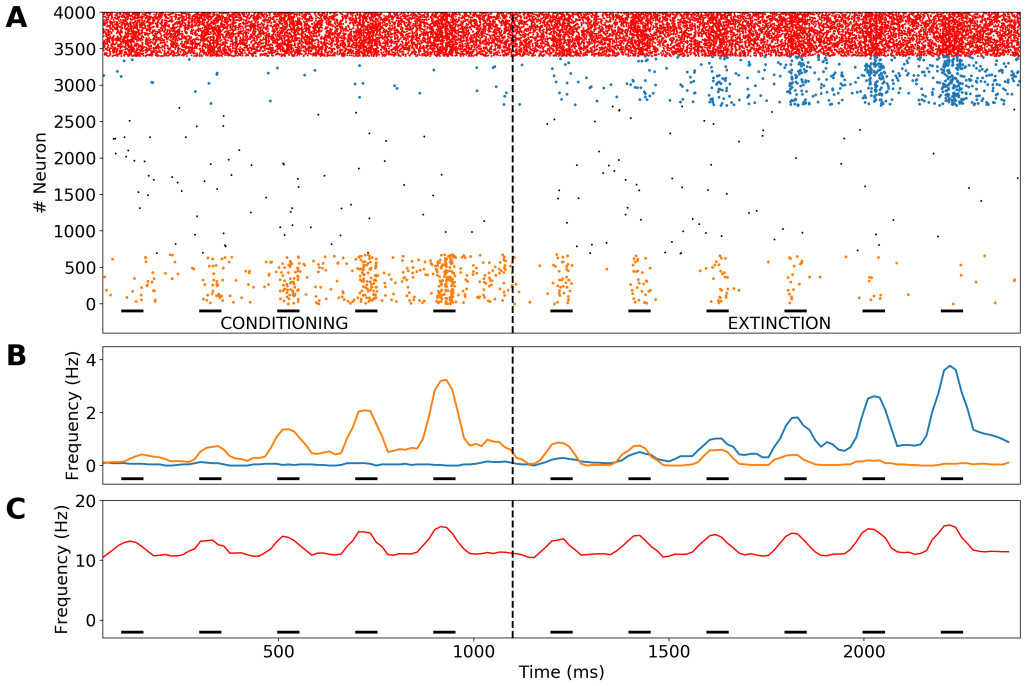

Figure 5. Dynamics of the spiking network model of BA. This figure should be compared to Figures 5**A**-**C** of the reference paper. (**A**) Raster plot of simulated spiking network activity during the conditioning and extinction phases. The amber and cyan dots represent pop_A and pop_B, respectively, while the red dots represent the inhibitory neuron population and the black dots represent the other excitatory neurons. (**B**) Firing rate per neuron of pop_A and pop_B (same colors as in **A**). (**C**) Firing rate per neuron of the inhibitory population. In (**B**) and (**C**) we used $\Delta t = 15$ ms. The loosely dashed horizontal lines symbolize the CS presentations during the simulation and the vertical dashed line marks the transition from conditioning to extinction phase.

In the caption of Figure 5 of the reference article, the authors explain that pop_A and pop_B, each one, corresponds to 50% of the total excitatory neurons. However, this is in disagreement with the methodology presented by them. In our study, we considered 20% of the total excitatory neurons for each subpopulation as described in the original methodology and shown in Figure 2.

We evaluated 30 simulations for the conditioning and extinction dynamics, and in all of them it was possible to verify the same scenario presented in Figure 5. In general, after each presentation of CS there is an increase in synaptic weights associated with the CTX applied followed by a decay when this CTX is inactivated. Thus, the results relative to the average firing rates and synaptic weights (Figure 6) are consistent as expected from the synaptic plasticity rules applied (Equation 8), and compatible with the original study.

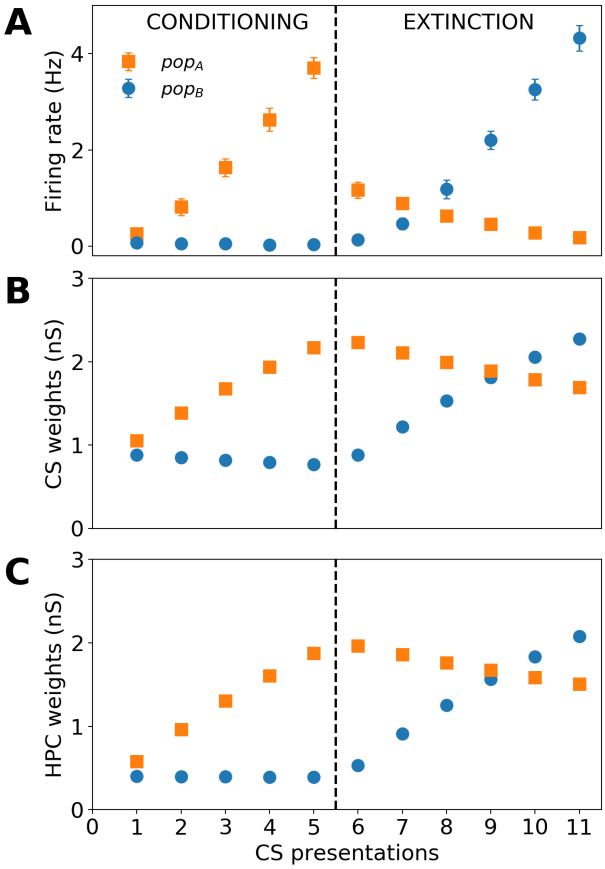

Figure 6. Figure to be compared to Figures 5**E-J** of the reference paper. (**A**) Evolution of the firing rates of pop_A and pop_B neurons during fear conditioning (left) and extinction (right). Firing rates were evaluated over 30 simulations. (**B**) Evolution of synaptic weights of CS inputs to pop_A and pop_B neurons during fear conditioning (left) and extinction (right). (**C**) Same as in (**B**) for the synaptic weights of CTX inputs during CS presentations. Here we chose to maintain the same acronym HPC used in the main reference, which refers to CTX.

Fear renewal — The results for these simulations are shown in Figures 7 and 8, and should be compared to Figures 7**A-C** and Figures 7**E-H** of the reference paper, respectively. In Figure 7**A** we show the spiking raster plot for the simulation, and in Figure 7**B-C** the activities of the excitatory and inhibitory populations, respectively. During the transition from the extinction to the renewal phase: i) the change of CTX causes a sudden modification in the firing rates of pop_A and pop_B neurons (Figures 7**B** and 8**A**); but ii) this effect barely influences the CS and CTX synaptic weights due to the synaptic plasticity rules (Figures 8**B** and 8**C**).
In accordance with the reference article, the rapid change in the activity of subpopulations is a network phenomenon and not an effect of synaptic plasticity, although it plays an important role in the whole dynamics that precedes the renovation. Additionally, we observed a slight change in CS and CTX weights in the transition from extinction to renewal, which might be related to the difference between the time constants used in our replication and the original model (this could indicate that our $\tau_{h/c}$ is slightly faster) to simulate the synaptic plasticity.

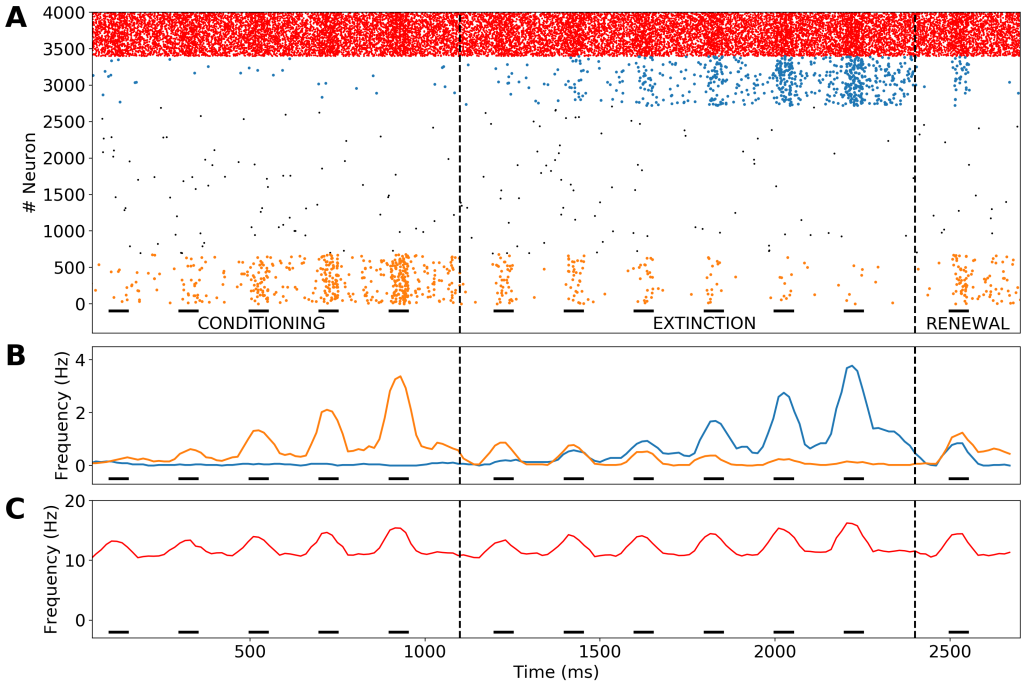

Figure 7. ABA fear renewal. This scenario is equivalent to that shown in Figure 5, with the reactivation of CTX_A and an additional presentation of CS. (**A**) Raster plot of spiking activity of fear (amber), extinction (cyan), inhibitory (red), and other excitatory (black) neurons. (**B**) Average firing rate of pop_A and pop_B neurons. (**C**) Average firing rate of the inhibitory neurons. Dashed horizontal lines symbolize the CS presentations during the simulation and dashed vertical lines mark the transitions between conditioning and extinction and extinction and renewal. The exchange of CTX after the extinction phase causes an instantaneous change in activity between pop_A and pop_B neurons. In (**B**) and (**C**) we used $\Delta t = 15$ ms.

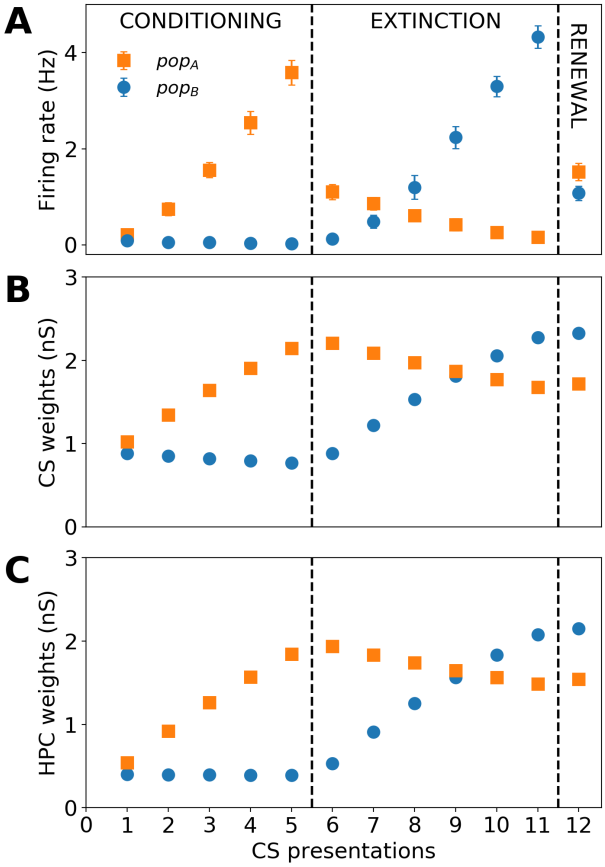

Figure 8. (**A**) Average firing rates of pop_A and pop_B neurons during conditioning, extinction and renewal. Averages were performed over 30 simulations of ABA renewal. (**B**) Synaptic weights of CS inputs to pop_A and pop_B neurons. (**C**) Synaptic weights of CTX inputs during CS presentations. Here we chose to maintain the same acronym HPC used in the reference article that refers to CTX. During renewal, the synaptic weights undergo slight changes because of the synaptic plasticity rule applied. Despite a decline in the synaptic weights of pop_A at the end of the extinction phase, these weights still have higher values than at the beginning of the conditioning phase, thus when reactivating the CTX_A, the firing rate for pop_A increases sharply. Note that in Figure 7F of the original article the colors used to indicated the populations are inverted.

High connectivity introduces gamma oscillations — In the corresponding section of the reference article, the connection probability p_{II} (defined here in Table 3) was increased to the experimentally reported value of 0.5 [10] to study the effect of this high connectivity on the behavior of the spiking network model. The authors reported that this change in the network did not affect the qualitative behavior of the model but a new aspect emerged in the dynamics: gamma oscillations in the network firing rate.
With a careful inspection of Figure 8A of the main reference, we noted that the authors studied this phenomenon only for the conditioning phase and, to obtain a similar result, we increase the amount of CS presentations to 10 (this result is dependent on the number of CS presentations). The results for this procedure are shown in Figure 9.

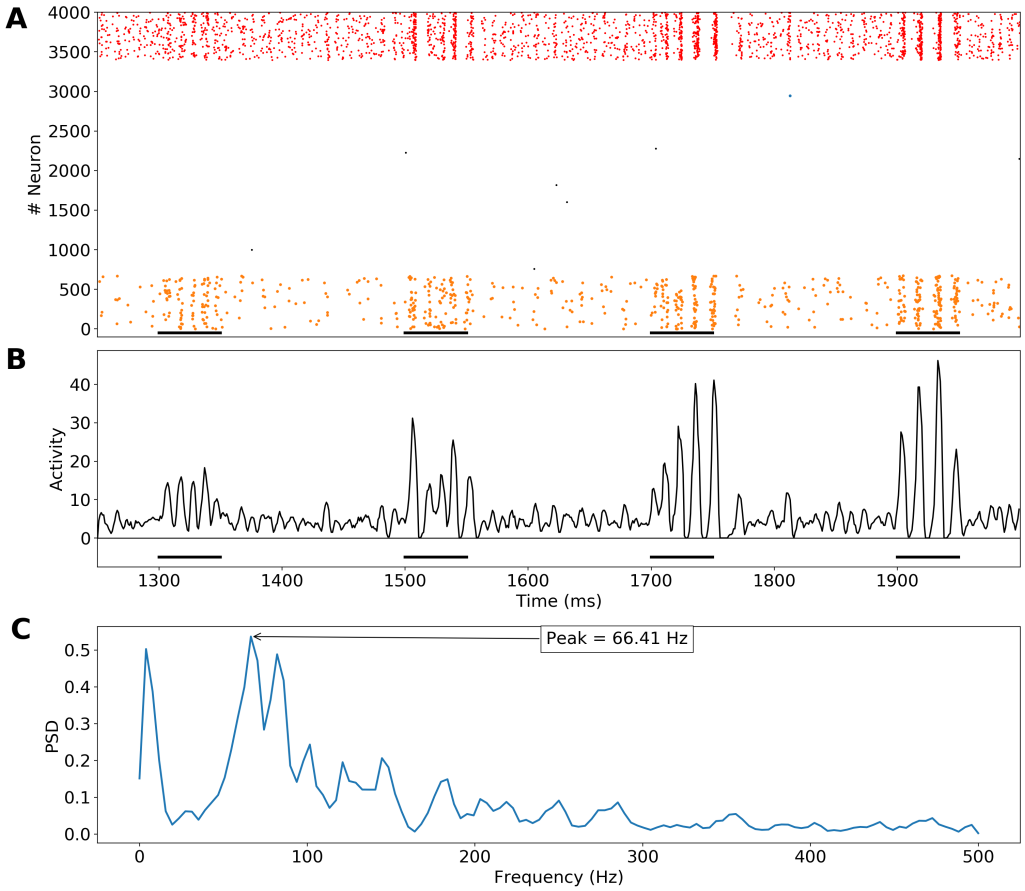

Figure 9. Gamma oscillations for high network connectivity. (**A**) Raster plot of spiking activity for the last 4 presentations of CS during the conditioning phase. Amber dots represent the fear neurons, red dots the inhibitory neurons, and black dots the other excitatory neurons. (**B**) Histogram (smoothed) of population activity. During each presentation of CS (horizontal black lines), it is possible to notice signatures of gamma oscillations. (**C**) Power spectrum density of the time series in (**B**). The peak at 66.41 Hz (in the gamma band) is indicated by an arrow.

In Figure 9A, we show a raster plot of the spiking activity for the last four CS presentations. At each presentation the neurons fire in a more synchronous fashion as can be seen in Figure 9B. The PSD of this synchronous activity is shown in Figure 9C and it displays a peak at 66.41 Hz, within the gamma oscillation range (30-80 Hz). Thus, through our approximation, we obtained a similar result to that observed in Figure 8A of the original work.
Further, the authors investigated how the network properties impact the overall synchrony. To illustrate the meaning of the synchrony index used in this replication, in Figure 10 we show time series of the synchrony index for three different types of activity

of the inhibitory population (obtained with different values of p_{II}). As gamma oscillations emerge, the synchrony index increases. In particular, we show that the oscillatory power of the network is positively correlated with the synchrony index. Specifically for this network the characteristic oscillations are always within the gamma band. We will assume that a synchrony index greater than 4.5 characterizes the presence of gamma oscillations.

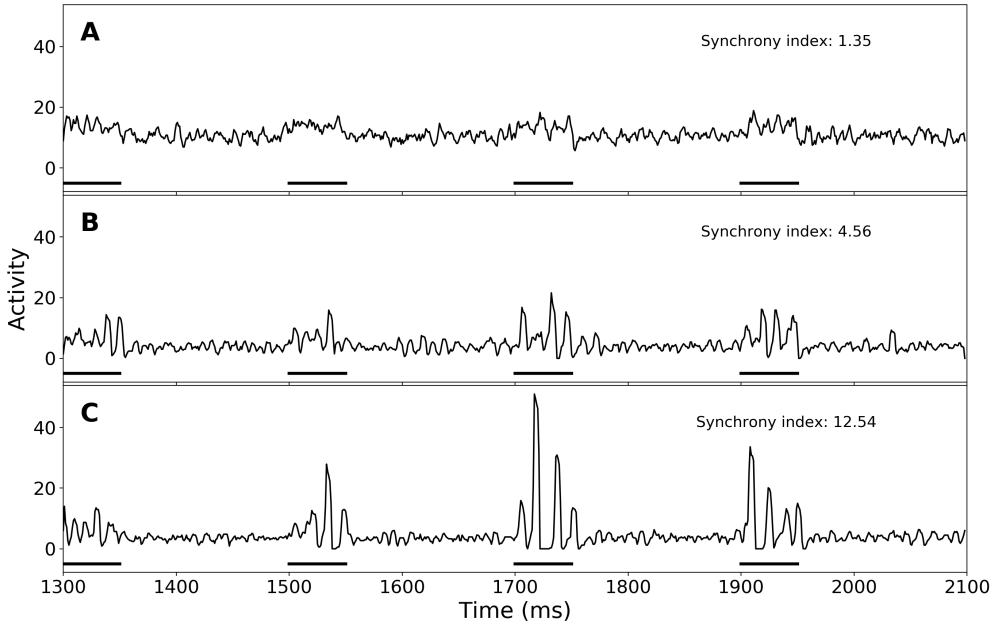

Figure 10. Synchrony index and gamma oscillations. (**A**) Non-synchronized case. (**B**) Synchronized case with emergence of gamma oscillations. (**C**) Synchronized case with strong gamma oscillations. The synchronization index shown above each plot was calculated using the activity of the inhibitory population obtained with a histogram of bin size $\Delta t = 1$ ms, delay distributed uniformly between $[1.0 - 2.0]$ for an inhibitory synaptic weight of 2 nS. The times series were generated with three different values of connection probability among inhibitory neurons: (**A**) $p_{II} = 0.1$, (**B**) $p_{II} = 0.6$, and (**C**) $p_{II} = 0.7$.

To explore mechanisms operating in BA that could dampen gamma oscillations, the authors of the original text investigated the measure of synchrony as a function of connectivity, synaptic weights and delays between inhibitory neurons. The p_{II} connectivity was analyzed from 0.1 to 0.9, at 0.1 intervals; synaptic weights w_{II} were set to 1, 2 or 3 nS; and delays were divided in two groups: "higher", uniformly distributed between $[1.0 - 2.0]$ ms, and "lower", uniformly distributed between $[0.2 - 1.0]$ ms.
Figure 11 shows the synchrony index for simulations with all possible combinations of these three groups of parameters. Gamma oscillations are not present (regions bellow the purple dashed line in Figure 11) for both delay scenarios ("higher" and "lower") when one of the following conditions is true: (i) p_{II} lower than 0.4, or (ii) $w_{II} = 1$ nS independently of p_{II}. For delay type "lower", there is a reduction of oscillations in all situations, which is compatible with the reference article. Thus, changes in the inhibitory structure of the network are essential to obtain gamma oscillations in neuronal activity.

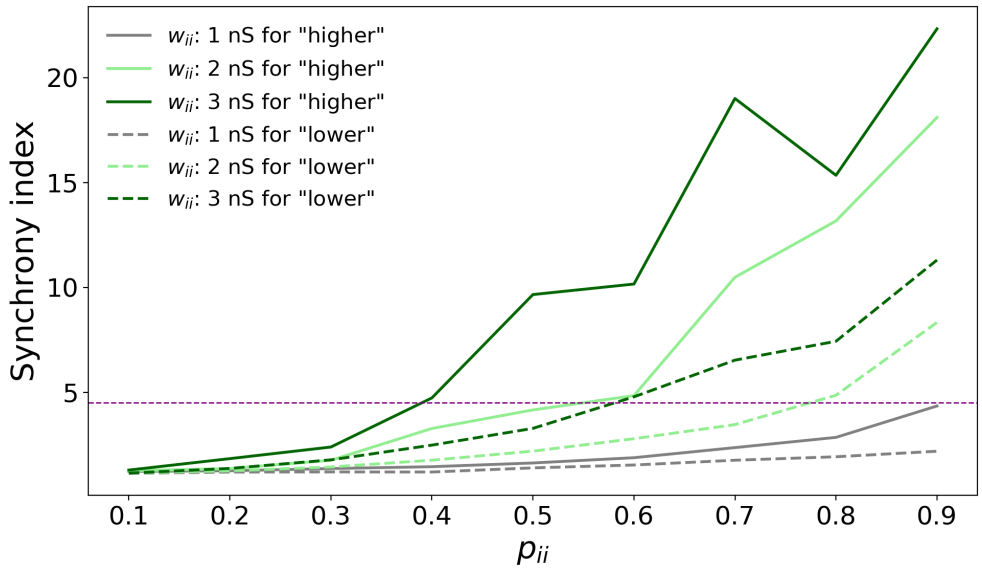

Figure 11. Effects of connectivity, synaptic weights and delays of the inhibitory population on synchronization. The synchrony index used was the Fano factor calculated on the histogram of inhibitory spikes during the presentation of the last four CS during the conditioning phase. The combinations between synaptic weights and delays are indicated by different colors (gray, light green and dark green) and line types (continuous or dashed) as indicated on the left-hand top corner. The purple dashed line indicates the threshold value 4.5 above which the synchrony index indicates gamma oscillations according to our definition.

Blockage of inhibition — Inhibition plays an important role in controlling the firing rate of the network as can be seen in Figure 5A, in which the firing rate of excitatory neurons not belonging to subpopulations A and B (black dots) remains close to zero even with presentations of CS. Based on this, we performed two additional sets of simulations where we deactivated first 50% and then 90% of inhibitory neurons during the extinction phase.

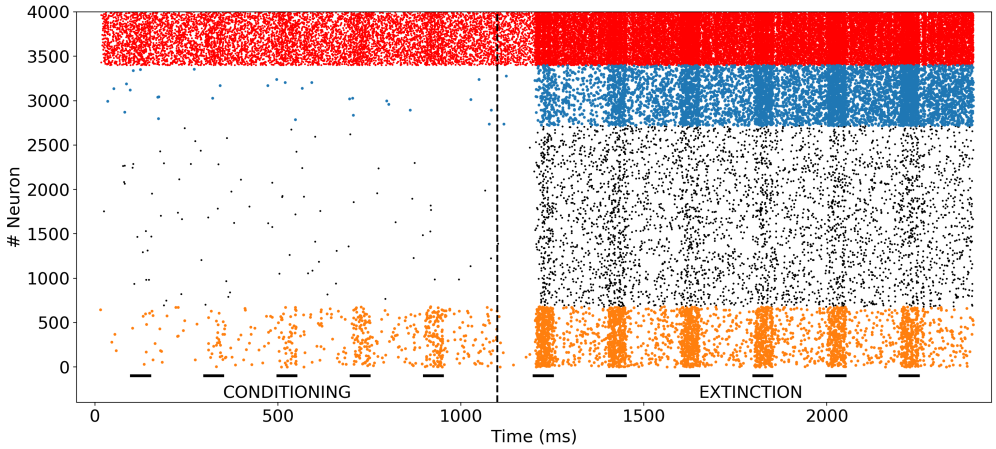

Figure 12. Blockage of 90% inhibitory activity during the extinction phase. The raster plot corresponds to the same situation (with the same color code) shown in Figure 5 with the difference that in the extinction phase we set to zero the synaptic weights for 90% of the inhibitory population. Although in our simulation these neurons fire, they do not affect other neurons.

In Figure 12, we show the raster plot of spiking neuronal activity for 90% of inhibitory blockage. The firing rates of all excitatory neurons are abruptly increased when inhibitory neurons are deactivated during CTX_B presentation. To underline this effect, in Figure 13 we show the firing rate during the last CS presentation (corresponding to Figure 8**C** of the original paper). As expected, the increase in the fraction of "blocked" inhibitory cells provokes an increase in the firing rate, and this effect is even stronger for the extinction neurons (pop_B). This suggests that if the relative difference between the activities of the fear and extinction neurons were crucial, extinction must be favored by the blockage of inhibition in this scenario.

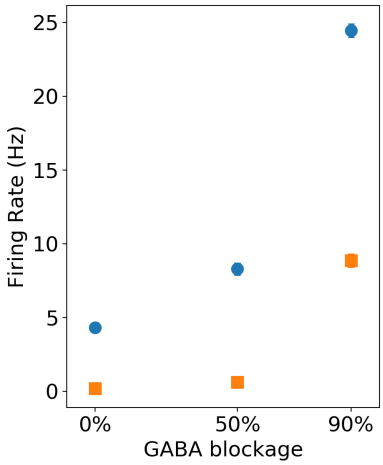

Figure 13. Blockage of inhibitory neurons during the extinction phase leads to an increase in the firing rates of pop_A (fear neurons, amber) and pop_B (extinction neurons, cyan). The relative difference between the firing rates also increases.

Conclusions

We replicated two models proposed by Vlachos et al. (2011) [2] to study aspects related to fear and extinction memories in the BA. These phenomena depend on the activation of two subpopulations of neurons for different context stimuli. The models were originally built in NEST and Matlab and here we reimplemented them using Python and Brian 2. Due to lack of some parameter values, data analysis details, and simulation protocols in the original article, we had to make some adaptations and successfully replicated the following results:

- for the mean-field model, the obtained result qualitatively replicates the original result.
- for the spiking network model, the results obtained are qualitatively consistent with the original work. In addition, we added descriptions and extra figures that help to understand all the methodological procedures adopted.

Even though we did not replicate all results of the original paper, the qualitative replication described here suffices to give support to the claim of the authors of the original article that their model captures the experimental observations.

Acknowledgements

This replication work started as a student project during the VIII Latin American School on Computational Neuroscience (LASCON 2020).
This article was produced as part of the activities of FAPESP Research, Innovation and Dissemination Center for Neuromathematics (Grant No. 2013/07699-0, S. Paulo Research Foundation). T.T.A.C. is supported by a scholarship from the National Council of Scientific and Technological Development (CNPq) (Grant No. 141579/2017-0) and Fundação de Amparo à Ciência e Tecnologia de Pernambuco (FACEPE) (Grant No. BFD-0013-1.05/20). The authors also thank FAPESP support through Grants Nos. 2015/50122-0, 2018/20277-0 (A.C.R.), 2016/03855-5 (N.L.K.) and 2017/07688-9 (R.O.S). V.L.C received a CAPES PhD scholarship and L.B.D a Capes MSc scholarship. A.C.R. thanks financial support from CNPq (Grant No. 306251/2014-0). This study was financed in part by the Coordenação de Aperfeiçoamento de Pessoal de Nível Superior - Brasil (CAPES) - Finance Code 001.

References

1. C. Herry, S. Ciocchi, V. Senn, L. Demmou, C. Müller, and A. Lüthi. "Switching on and off fear by distinct neuronal circuits." In: **Nature** 454 (2008), pp. 600–606.
2. I. Vlachos, C. Herry, A. Lüthi, A. Aertsen, and A. Kumar. "Context-dependent encoding of fear and extinction memories in a large-scale network model of the basal amygdala." In: **PLoS Comput. Biol.** 7 (2011), e1001104.
3. M.-O. Gewaltig and M. Diesmann. "NEST (NEural Simulation Tool)." In: **Scholarpedia** 2.4 (2007), p. 1430.
4. M. Stimberg, R. Brette, and D. F. Goodman. "Brian 2, an intuitive and efficient neural simulator." In: **eLife** 8 (Aug. 2019).
5. H. R. Wilson and J. D. Cowan. "Excitatory and inhibitory interactions in localized populations of model neurons." In: **Biophys. J.** 12 (1972), pp. 1–24.
6. A. Kumar, S. Schrader, A. Aertsen, and S. Rotter. "The high-conductance state of cortical networks." In: **Neural Comput** 20 (2008), pp. 1–43.
7. P. Sah, E. S. L. Faber, M. Lopez de Armentia, and J. M. J. P. R. Power. "The amygdaloid complex: anatomy and physiology." In: **Physiol. Rev.** 83 (2003), pp. 803–834.
8. D. Golomb and J. Rinzel. "Dynamics of globally coupled inhibitory neurons with heterogeneity." In: **Phys. Rev. E** 48 (1993), pp. 4810–4814.
9. D. Golomb. "Neuronal synchrony measures." In: **Scholarpedia** 2.1 (2007), p. 1347.
10. A. R. Woodruff and P. Sah. "Networks of parvalbumin-positive interneurons in the basolateral amygdala." In: **J. Neurosci.** 27 (2007), pp. 553–563.